Imaging, Diagnosis, Prognosis

Clinical Cancer Research

In Vivo Imaging of Prostate Cancer Using [^{68}Ga]-Labeled Bombesin Analog BAY86-7548

Esa Kähkönen[1], Ivan Jambor[5,6], Jukka Kemppainen[2,5], Kaisa Lehtiö[3], Tove J. Grönroos[5], Anna Kuisma[3], Pauliina Luoto[5], Henri J. Sipilä[5], Tuula Tolvanen[5], Kalle Alanen[4], Jonna Silén[5], Markku Kallajoki[4], Anne Roivainen[5], Niklaus Schäfer[7,8], Roger Schibli[9], Martina Dragic[9], Anass Johayem[8], Ray Valencia[10], Sandra Borkowski[10], and Heikki Minn[3,5]

Abstract

Purpose: A novel [^{68}Ga]-labeled DOTA-4-amino-1-carboxymethyl-piperidine-*D*-Phe-Gln-Trp-Ala-Val-Gly-His-Sta-Leu-NH_2 peptide (BAY86-7548) having high affinity to bombesin receptor subtype II to detect primary and metastatic prostate carcinoma using positron emission tomography/computed tomography (PET/CT) was synthesized and evaluated for prostate cancer.

Experimental Design: In this first human study with BAY86-7548, 14 men scheduled for radical prostatectomy ($n = 11$) or with biochemical recurrence after surgery or hormonal therapy ($n = 3$) were enrolled. The patients received an intravenous injection of BAY86-7548 followed by over 60-minute dynamic imaging of prostate gland ($n = 10$) and/or subsequent whole-body imaging ($n = 14$). The visual assessment of PET/CT images included evaluation of intraprostatic (12 subsextants) and pelvic nodal uptake of BAY86-7548 in 11 surgical patients and detection of potential metastatic foci in all patients. In patients with biochemical recurrence, results were compared with those of either [^{11}C]-acetate ($n = 2$) or [^{18}F]-fluoromethylcholine ($n = 1$) PET/CT.

Results: We found a sensitivity, specificity, and accuracy of 88%, 81% and 83%, respectively, for detection of primary PCa and sensitivity of 70% for metastatic lymph nodes using histology as gold standard. BAY86-7548 correctly detected local recurrence in prostate bed and showed nodal relapse in accordance with [^{11}C]-acetate PET/CT in 2 patients with biochemical relapse. In the third hormone refractory patient, BAY86-7548 failed to show multiple bone metastases evident on [^{18}F]-fluoromethylcholine PET/CT.

Conclusion: BAY86-7548 PET/CT is a promising molecular imaging technique for detecting intraprostatic prostate cancer. *Clin Cancer Res; 19(19); 5434–43. ©2013 AACR.*

Introduction

Prostate cancer is the most frequently diagnosed cancer and the second most common cause of cancer-related deaths among men (1). Prostate-specific antigen (PSA) and digital rectal examination are the first-line investigations in evaluating the risk of prostate cancer, whereas diagnosis is mainly based on transrectal ultrasound (TRUS)–guided biopsies. Because of low diagnostic accuracy of TRUS, many doctors prefer systematic biopsies for detection of prostate cancer (2). However, about 25% to 35% of cancers are missed on first systematic biopsy (3, 4) and the Gleason score, which characterizes the malignant potential of prostate cancer, is commonly underestimated (5). In addition, attempts to improve prostate cancer detection by intensifying the biopsy technique have failed and seem to increase the risk of complications (6). Therefore, better imaging tools are needed to detect clinically significant cancer foci and to avoid unnecessary biopsies. Moreover, precise localization of cancer is needed to improve and further develop local prostate gland sparing therapies.

Multiparametric MRI has been shown to improve diagnostic accuracy in the evaluation of intraprostatic prostate cancer (7). Nevertheless, due to different imaging protocols, technical factors, and study populations, the variability in

Authors' Affiliations: [1]Department of Surgery, Division of Urology, Departments of [2]Clinical Physiology and Nuclear Medicine, [3]Oncology and Radiotherapy, and [4]Pathology, Turku University Hospital; [5]Turku PET Centre; [6]Department of Diagnostic Radiology, University of Turku, Turku, Finland; Departments of [7]Medical Oncology and [8]Nuclear Medicine, University Hospital of Zurich; [9]Department of Chemistry and Applied Biosciences, ETH Zurich, Zurich, Switzerland; [10]Bayer Pharma AG, Berlin, Germany

E. Kähkönen and I. Jambor contributed equally to this article.

Prior presentation: Part of the study was presented at the 25th European Association of Nuclear Medicine (EANM) Annual Meeting in Milan on October 27–31, 2012 and Radiological Society of North America (RSNM) Annual Meeting in Chicago, November 25-December 1, 2012.

Corresponding Author: Heikki Minn, Department of Oncology and Radiotherapy, Turku University Hospital, Kiinamyllynkatu 4-8, P.O. Box 52, FI-20521 Turku, Finland. Phone: 358-2-313-0149; Fax: 358-2-313-2809; E-mail: heminn@utu.fi

doi: 10.1158/1078-0432.CCR-12-3490

Translational Relevance

Overexpression of bombesin receptors has been observed in several neoplastic diseases, including prostate cancer, thus offering a promising target for *in vivo* imaging. Anatomic imaging often fails to detect local disease with sufficient specificity for emerging focal therapies for prostate cancer. Therefore, novel techniques showing the dominant intraprostatic lesion are becoming increasingly important. This study shows that ^{68}Ga-labeled DOTA-4-amino-1-carboxymethyl-piperidine-*D*-Phe-Gln-Trp-Ala-Val-Gly-His-Sta-Leu-NH_2-peptide (BAY86-7548) positron emission tomography/computed tomography (PET/CT) detects organ-confined prostate cancer with an accuracy of 83%, which is at least comparable with multiparametric MRI and PET/CT using radiolabeled choline or acetate. Autoradiography (ARG) findings obtained from surgical specimens indicated that BAY86-7548 indeed detects bombesin receptor subtype II (gastrin-releasing peptide receptor; GRPr)–positive lesions and could assist in planning of focal treatment of prostate cancer.

the reported sensitivities and specificities remains high (7, 8).

PET is frequently used in oncology but its role in diagnosis of primary prostate cancer is not well established. The most common tracer, 2[^{18}F]fluoro-2-deoxy-D-glucose (FDG), has a low sensitivity for detecting early prostate cancer due to the low glucose consumption (9, 10), limiting the possibility to detect clinically localized disease. Other tracers, such as ^{18}F- or ^{11}C-labeled choline and [^{11}C]-acetate, are used mainly for the diagnosis of recurrent (11–13) or metastatic (14) prostate cancer. Their feasibility in primary diagnosis is limited because of uptake in benign tissue such as benign prostatic hyperplasia (BPH; refs. 15, 16).

^{68}Ga-labeled DOTA-4-amino-1-carboxymethyl-piperidine-*D*-Phe-Gln-Trp-Ala-Val-Gly-His-Sta-Leu-NH_2 (BAY86-7548) is a synthetic bombesin receptor antagonist, which targets gastrin-releasing peptide receptors (GRPr; ref. 17). GRPr proteins are highly overexpressed in several human tumors, including prostate cancer (18). Because of their low expression in BPH and inflammatory prostatic tissues (19, 20), imaging of GRPr has potential advantages over current choline- and acetate-based radiotracers. Indeed, preclinical studies using BAY86-7548 have shown a high and persistent tracer uptake in mice bearing PC-3 tumor xenografts, which represent androgen-independent human prostate cancer with high GRPr expression (21).

The aim of this prospective, multisite study was to investigate the safety, tolerability, and accuracy of BAY86-7548 in detection of primary prostate cancer and lymph node metastases in patients scheduled for radical retropubic or robot-assisted laparoscopic prostatectomy. In addition, feasibility of detecting recurrent prostate cancer in comparison with [^{18}F]-fluoromethylcholine, [^{11}C]-acetate positron emission tomography/computed tomography (PET/CT), or MRI was examined in 3 patients with increasing PSA after radical or palliative treatment. Finally, the potential of BAY86-7548 to study GRPr expression in human prostate cancer was studied.

Materials and Methods

Patients and study design

Eleven patients (mean age, 63 years; range, 48–72 years) with histologically confirmed prostate adenocarcinoma, diagnosed through systematic TRUS-guided biopsies, and 3 patients (mean age, 67 years; range, 51–82 years) with biochemical recurrence of prostate cancer were prospectively enrolled. Individual patient characteristics are presented in Table 1. Thirteen patients were studied in Turku, Finland and 1 patient was studied in Zurich, Switzerland. Additional inclusion criteria for patients undergoing radical prostatectomy were presence of cancer in at least 20% of biopsy material and patient preference to undergo radical surgery including pelvic lymphadenectomy after discussion of the treatment options with the study urologist (E. Kähkönen). None of the patients studied in Turku had received any hormonal therapy or radiotherapy, whereas the patient in Zurich was in androgen-resistant phase after pelvic radiotherapy, several local palliative radiotherapies, and antiandrogenic therapy. In addition, a multiparametric 3T MRI using surface coil was conducted for 3 patients (no. 9, 11, and 12) and [^{11}C]-acetate PET/CT in 3 patients (no. 11, 12, and 13). The patient in Zurich (no. 14) underwent [^{18}F]-fluoromethylcholine PET/CT. Multiparametric 3T MRI consisted of anatomic T2- and T1-weighed images, dynamic contrast–enhanced MRI, and diffusion-weighed imaging.

The study protocol was approved by the local ethics committees in Turku and Zurich as well as the respective authorities and each patient gave written informed consent for participation in the study. The entire study was carried out according to the guidelines of the Declaration of Helsinki.

Synthesis of BAY86-7548

The precursor, DOTA-4-amino-1-carboxymethylpiperidine-*D*-Phe-Gln-Trp-Ala-Val-Gly-His-Sta-Leu-NH_2 (BAY86-7547), was obtained from Bayer HealthCare Pharmaceuticals. All the other reagents were purchased from commercial suppliers and were synthesized or analytically graded.

Turku. The radiosynthesis was conducted with fully automated synthesis device (Modular Lab, Eckert & Ziegler Eurotope GmbH). ^{68}Ga was obtained from a ^{68}Ge/^{68}Ga generator [IGG-100; 50 mCi (1,850 MBq); Eckert & Ziegler Isotope Products] by eluting the generator with 7 mL of 0.1 mol/L HCl. The radioactive fraction of the ^{68}Ga eluate (1.6 mL) was collected and the HEPES–buffered BAY86-7547 (28 μg; 17 nmol) was added. The reaction mixture was incubated at 100°C to 120°C for 12.5 minutes followed by SepPak purification, sterile filtration, and formulation with sterile PBS. The identity and the radiochemical purity of the

Table 1. Patient characteristics

Patient no.	Age, y	Injected radioactivity, MBq	Postoperative TNM	Prostate gland weight, g	Gleason score[c]		PSA at imaging, ng/mL	Preoperative risk of N+ disease, %	No. of PCa lesions	Size of dominant lesion, mm	Proportion of cancer in prostate gland, %	No. of metastatic/ recovered lymph nodes	Setting[a]
					ARG, right/left	Final							
1	62	161	T3bN1	54	0/3+4	4+3	16	30	2	17	30	1/15	P
2	57	160	T3aN0	59	3+3/3+4	3+4	6.9	7	3	16	30	0/14	P
3	72	150	T3bN0	152	3+3/3+3	4+3	45	28	2	26	20	0/3	P
4	69	159	T3bN0	55	0/4+4	3+4	21	60	1	19	20	0/7	P
5	63	154	T3aN0	47	3+4/3+3	4+3	6.2	17	2	16	20	0/13	P
6	62	153	T3bN1	35	3+3+4+4	4+4	15	22	3	12	20	3/13	P
7	64	148	T2cN0	32	3+4/4+3	3+4	17	22	1	35	20	0/20	P
8	66	146	T4N1M1	54	5+4/5+4	5+4	14	33	1	32	60	6/17	P
9	66	158	T3aN0	101	0/0	4+3	13	26	2	12	7	0/8	P
10	48	147	T2cN0	32	0/3+4	3+4	10	16	1	22	25	0/15	P
11	64	129	T3aN0	66	N/A[b]	4+4	29	78	1	20	10	0/10	P
12	52	143	T3bN0M0	N/A[b]	N/A[b]	4+4	0.36	N/A[b]	N/A[b]	N/A[b]	N/A[b]	N/A[b]	R
13	67	108	T2cN0M0	N/A[b]	N/A[b]	4+5	4.7	N/A[b]	N/A[b]	N/A[b]	N/A[b]	N/A[b]	R
14	82	152	T2N1M0	N/A[b]	N/A[b]	2+3	282	N/A[b]	N/A[b]	N/A[b]	N/A[b]	N/A[b]	R
Mean	64	147											
SD	8	15											

Abbreviations: PCa, prostate cancer; TNM, tumor—node—metastasis.

[a]P, primary cancer, R, recurrence.

[b]N/A, not applicable.

[c]Final Gleason score is based on the whole-mount prostatectomy, whereas ARG Gleason score is from the particular tissues section used for ARG.

product (BAY86-7548) were evaluated by radio-high-performance liquid chromatography (radio-HPLC). The identity was confirmed by comparing the retention times of the peaks obtained from BAY86-7548 and BAY86-7547. The *in vitro* stability of BAY86-7548 was tested in formulation solution (PBS) by incubating for 2 hours at room temperature followed by radio-HPLC analysis.

Zurich. The radiosynthesis was comparable with that in Turku except for the ^{68}Ga eluate, which was trapped onto a cation-exchange cartridge (Strata-X-C, Phenomenex). Then, 0.4 mL of 98% acetone/0.02 mol/L HCl was used to elute ^{68}Ga from the cartridge. The peptide BAY86-7547 (28 μg; 17 nmol) and uric acid were dissolved in 2 mL of 0.2 mol/L sodium acetate buffer and were prefilled into the reaction vessel. This was followed by incubation of the reaction mixture at 95°C for 6 minutes and 40 seconds, and formulation and *in vitro* stability testing was carried out in saline instead of PBS. Otherwise, the procedures were similar.

BAY86-7548 PET/CT imaging

The patients were imaged in supine position using a GE Discovery VCT (Turku) or ST16 (Zurich) PET/CT Scanner (General Electric Medical Systems). Low-dose CT protocol (120 kV, 10–80 mA, noise index 25, slice thickness, 3.75 mm in Turku; and 140 kV, 10–80 mA, noise index 11.75, slice thickness, 3.75 mm in Zurich) was conducted and also used for attenuation correction. A median dose of 147 MBq (range, 108–161 MBq) of BAY86-7548 was injected as an intravenous bolus. During imaging, the vital signs were monitored including a 12-lead electrocardiogram, and blood and urine chemistry. The measured data were corrected for dead time, decay, and photon attenuation and reconstructed into 256 × 256 matrix. Image reconstruction followed a fully three-dimensional VUE Point GE algorithm incorporating random and scatter correction with two iterations and 28 subsets. The postfilter was 3.00 mm FWHM (full-width at half-maximum) and the field of view diameter was 700 mm yielding to image pixel size of 3 mm. The final in-plane resolution of both PET/CT systems was 5 mm.

Surgical patients (n = 11). Urethral catheter was used in 9 (82%) patients to limit accumulation of BAY86-7548 in bladder and to allow better visualization of urethra on PET/CT images. Tracer injection was immediately followed by dynamic PET acquisition of the lower pelvic area over 60 minutes in 10 patients. A static whole-body emission scan (seven bed positions, 420 seconds per bed position) covering the whole torso in caudal to cephalic direction was then acquired 69 ± 3 minutes after tracer injection. In addition, 6 patients had a second static PET of pelvic area (one bed position of 420-second duration) 102 ± 7 minutes after injection. Patient no. 1 had static PET emission scan covering pelvic area for 58 minutes after injection immediately followed by whole-body imaging.

Biochemical recurrence (n = 3). Two patients with suspicion of recurrent prostate cancer (nos. 12 and 13) had static PET emission scan covering whole-body for 58 minutes after tracer injection. The third patient with suspicion of bone metastases (no. 14) received whole-body imaging starting 60 minutes after injection.

BAY86-7548 PET/CT image analysis

An experienced nuclear medicine physician (J. Kemppainen) and a medical student (I. Jambor) interpreted the PET/CT images in Turku in consensus. Both examiners were aware of the prostate cancer diagnosis or suspicion of cancer recurrence, but were blinded to clinical and histopathologic findings. PET/CT images in Zurich were interpreted by an experienced nuclear medicine physician (N. Schäfer). In patients with primary prostate cancer, a region-based analysis was used. The prostate gland was divided into three parts in superior–inferior axis. Each third was further divided into four quadrants (anterior, posterior, left, and right). Presence of prostate cancer on PET/CT images was defined as any mono- or multifocal uptake greater than adjacent background in more than one slice within the CT-defined prostate gland area. In addition to region-based analysis, lesion-based analysis was conducted in which each abnormal focus was correlated with prostatectomy findings to define its histopathologic nature. Finally, regions of interest (ROI) were placed on visually identified abnormal foci as well as areas defined as BPH and normal prostate tissue of the peripheral zone based on histopathologic findings from whole-mount prostatectomy samples. Maximum standardized uptake value (SUV_{max}) and mean SUV with a 60% threshold (SUV_{mean}) were determined in all ROIs. Tumors with the largest diameter of more than 0.5 cm were included in the analysis. The diagnostic accuracy of BAY86-7548 PET/CT was assessed using whole-mount prostatectomy sections. In patients with biochemical recurrence, additional imaging modality was conducted to clarify the findings of BAY86-7548 PET/CT.

Surgery

Open radical retropubic ($n = 2$) or robot-assisted laparoscopic prostatectomy ($n = 9$) and bilateral extended iliacal lymphadenectomy was conducted 4 to 34 days after BAY86-7548 imaging. Preoperative risk of lymph node metastasis was estimated using Briganti nomograms (22). The surgeon (E. Kähkönen) was aware of the result of BAY86-7548 imaging and was encouraged to harvest especially the PET/CT–positive lymph nodes. The routine area resected was defined as follows: lateral border of excised fibrofatty tissue was pelvic wall and external and common iliac artery to the ureteral crossing, medial border was perivesical fat, inferior border was femoral canal, and superior border was ureter. In addition, the fibrofatty tissue from both obturator fossa and next to internal iliac artery was removed. Patient no. 3 had incomplete lymphadenectomy due to cardiopulmonary instability at the end of operation. Patient no. 8 showed suspicious metastatic lymph nodes outside routine lymphadenectomy area, just above aortic bifurcation on BAY86-7548 PET/CT and also had these nodes resected. These nodes were not detected on preoperative CT.

Histopathologic analysis

Histologic slides were analyzed by two experienced pathologists (K. Alanen and M. Kallajoki). After radical prostatectomy, the prostate glands were fixed in 10% buffered formalin for 24 to 48 hours. After fixation, the left, right, and anterior surfaces were inked with different colors to preserve the orientation of the prostate gland and to allow correlation with PET/CT images. Whole-mount axial macrosections were obtained at 8-mm intervals transversely in a plane perpendicular to the long axis of the prostate gland in superior–inferior direction. The most apical macrosection was further sectioned in coronal orientation for easier evaluation of the capsular status of the inferior region. The first transversal section at the base was further sectioned in sagittal orientation for easier evaluation of the margin and seminal vesicles. Four micrometer whole-mount sections from each macrosection were stained with hematoxylin and eosin. The presence and location of cancer foci, high-grade prostate intraepithelial neoplasm (HGPIN), prostatitis, BPH, capsular status, and seminal vesicle invasion were determined. Gleason score was assessed as combination of the most common and the second-most common type of Gleason grading for each tumor focus.

GRP receptor ARG

Fresh tissue samples of 1.5 cm × 1.5 cm × 0.5 cm size for ARG were taken from right and left lobe of prostate gland in 10 patients. Patient no. 2 had two fresh tissue samples from each lobe, whereas the remaining patients had only one per each lobe. The samples were immediately frozen at −70°C. Cryostat sections (20-μm thick) of these samples were processed for receptor ARG as described previously for other peptide receptors (22) using GRPr-specific [^{125}I]-Tyr^4-bombesin as radioligand (23). Tissue sections were mounted on precleaned microscope slides and stored at −20°C for at least 3 days to improve adhesion of tissue to the slide. Sections were then processed according to Vigna and colleagues. (23). They were first preincubated in 10 mmol/L of HEPES buffer (pH 7.4) for 5 minutes at room temperature followed by incubation in 10 mmol/L of HEPES, 130 mmol/L of NaCl, 4.7 mmol/L of KCl, 5 mmol/L of $MgCl_2$, 1 mmol/L of ethyleneglycol-bis (βb-aminoethylether)-N-N9-tetraacetic acid, 0.1% bovine serum albumin (BSA), 100 mg/mL of bacitracin (pH 7.4), and approximately 100 pmol/L of [^{125}I]-Tyr^4-bombesin-14 (81.4 TBq/mmol; PerkinElmer) in the presence or absence of 1 mmol/L of bombesin for 1 hour at room temperature. After incubation, the sections were washed four times for 2 minutes in 10 mmol/L of HEPES with 0.1% BSA (pH 7.4) at 4°C. Finally, the slides were rinsed twice for 5 seconds at 4°C in distilled water, dried at room temperature, and placed in apposition to imaging plates (Fuji Imaging Plate BAS-TR2025; Fuji Photo Film Co. Ltd.) for 14 days for scanning with the Fuji Analyzer FLA-5100. Sections were stained with hematoxylin and eosin to localize the areas of BPH, prostate cancer, and HGPIN.

Statistical analysis

Statistical analysis was conducted with SAS, version 9.3 (SAS Institute Inc.). SUV measurements were compared using Bonferroni multiple comparison test (24). Normal distributions were assessed by the Kolmogorov and Smirnov method. A P value below 0.01 was considered to be statistically significant.

Results

Patients' clinical findings are summarized in Table 1. No drug-related adverse events were associated with BAY86-7548 and all patients tolerated the imaging procedure well. The mean PSA level of patients with primary prostate cancer was 18 ± 11 ng/mL (range, 6.2–45.0 ng/mL), whereas the 3 patients with biochemical recurrence of prostate cancer had PSA levels of 0.36, 4.7, and 282 ng/mL. On the basis of histopathologic analysis of whole-mount prostatectomy samples, 26 tumor foci were identified in 11 patients, with 19 (73%) of these foci larger than 0.5 cm.

BAY86-7548 showed fast excretion through kidneys with 25% of injected radioactivity dose observed in urine 30 minutes after injection. Plasma pharmacokinetics, whole-body distribution, metabolism, and radiation dosimetry of BAY86-7548 in healthy men have been previously described (25). The highest radioactivity uptake was detected in the urinary bladder and pancreas, which is in the line with the known expression of GRPr and previous preclinical studies with RM2 peptide (21). Maximum peak uptake of the total injected radioactivity was seen in the urinary bladder and liver, 36% and 19%, respectively.

Preparation of BAY86-7548

The radiopharmaceutical BAY86-7548 was obtained with a moderate yield (440 ± 120 MBq; $n = 13$). Radioactivity concentration and specific radioactivity at end of synthesis (EOS) were 44 ± 13 MBq/mL and 26 ± 7 GBq/μmol, respectively. Radiochemical purity was at least 97% and the difference between retention times of HPLC peaks obtained from BAY86-7547 and BAY86-7548 was 0.19 ± 0.07 minutes. The tracer remained radiochemically stable for 2 hours in formulation solution at room temperature; radiochemical purity was 98% ± 0% at 1 hour after EOS and 98% ± 1% at 2 hours after EOS (mean ± SD; $n = 3$). Every injected batch of BAY86-7548 fulfilled the release criteria.

Diagnostic accuracy of cancer detection

Region-based analysis of BAY86-7548 PET/CT findings in 132 regions, of which 57 (43%) contained cancer according to histopathologic analysis, revealed 63 regions as positive and 69 as negative. Using histology as gold standard, 49 of these were considered true-positive and 61 true-negative, yielding a sensitivity, specificity, and accuracy of 89%, 81%, and 83%, respectively. Lesion-based analysis of BAY86-7548 PET/CT revealed 15 true-positive tumor lesions, 6 false-positive lesions, and 4 false-negative lesions resulting in a sensitivity of 79%. The 6 false-positive intraprostatic lesions were determined to be BPH based on whole-mount

prostatectomy sections. BAY86-7548 PET/CT successfully detected all dominant lesions except one anterior lesion. However, another smaller peripheral zone tumor of the same patient (no. 2) was detected. Both of the lesions had the Gleason score of 3+4.

Detection of lymph node metastasis

Primary prostate cancer with at least one metastatic lymph node was present in 3 (27%) of 11 patients undergoing prostatectomy with lymph node dissection. In total, 135 lymph nodes were histopathologically analyzed with 10 showing the presence of metastatic prostate cancer. Per patient sensitivity was 67% and per node sensitivity was 70% for BAY86-7548 PET/CT. The sizes of the three BAY86-7548–negative metastases were 6 (patient no. 1, left iliac node), 5, and 5 mm (patient no. 6, two right iliac lymph nodes). Patient no. 6 had in addition one correctly detected metastatic left iliac node (size 11 mm). Two normal-sized lymph nodes (less than 10 mm) were removed from patient no. 8 above the aortic bifurcation based on guidance of BAY86-7548 PET/CT (see section Surgery). Both of these were histopathologically confirmed as prostate cancer metastases (Fig. 1).

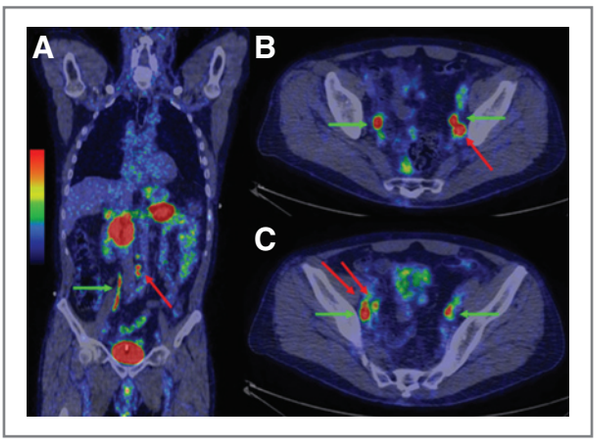

Figure 1. Coronal (A) and axial views (B and C) of BAY86-7548 PET/CT in patient no. 8 with prostate cancer metastasis to multiple lymph nodes. Two normal-sized (less than 10 mm) nodes above the aortic bifurcation indicated with red arrow showed increased uptake of tracer, SUV_{max} 6.2 and 6.3. In addition, one left parailiac node, SUV_{max} 12.7, (B) and two right parailiac nodes, SUV_{max} 6.1 and 4.7, (C) showed increased uptake of BAY86-7548. These five lymph nodes were histologically confirmed as metastases at surgery. Green arrows point to ureters, which can be easily distinguished on anatomic CT. Images are scaled to SUV, with a minimum at 0 and maximum at 5.

Quantitative analysis

The average SUV_{max} and SUV_{mean} were 6.6 ± 4.7 and 5.1 ± 3.7, respectively, for histologically confirmed cancer foci as measured 60 to 70 minutes after injection. These values were different from the SUV_{max} and SUV_{mean} of BPH (2.4 ± 1.5 and 1.8 ± 1.2, respectively) and normal tissue of peripheral zone (1.3 ± 1.0 and 1.0 ± 0.9, respectively; $P < 0.01$ for all comparisons). No significant difference in SUV_{max} and SUV_{mean} of BPH and normal tissue of peripheral zone was observed (see Fig. 2).

Results of ARG

Prostate cancer was present in 15 (68%) ARG sections. All lesions were positive by ARG. BPH nodules in two tissue sections and HGPIN lesion in one tissue section were positive, indicating the presence of GRPr expression (Fig. 3).

Patients with clinical suspicion of recurrent disease

BAY86-7548 PET/CT successfully detected recurrence of prostate cancer in the two hormone-naïve patients with biochemical recurrence (no. 12 and 13). The findings were in concordance with [^{11}C]-acetate PET/CT and 3T MRI in prostate bed in patient no. 12. In contrast, both [^{11}C]-acetate PET/CT and diffusion-weighted MRI suggested the presence of metastatic parailiac lymph node, whereas BAY86-7548 PET/CT did not show any pathologic uptake in this region. The patient subsequently received radiotherapy for PET- and MRI-positive prostatic bed and parailiac nodes bilaterally. In a repeated [^{11}C]-acetate PET/CT 3 months from radiotherapy, PSA was 0.068 and the prostate bed had turned [^{11}C]-acetate negative, whereas the parailiac lymph node was still positive. On CT, this node measured 6 mm and remained unchanged before and after

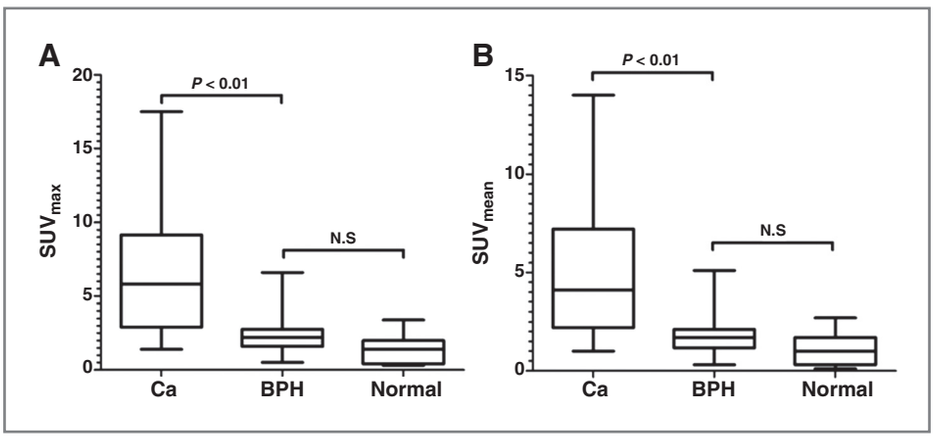

Figure 2. Maximum (A) and mean (B) SUV of BAY86-7548 in carcinoma, BPH, and normal prostate gland tissue in 11 patients scheduled for radical prostatectomy. Significantly higher uptake expressed as SUV_{max} and SUV_{mean} of cancer foci was found compared with both BPH and normal tissue of peripheral zone. N.S., not significant.

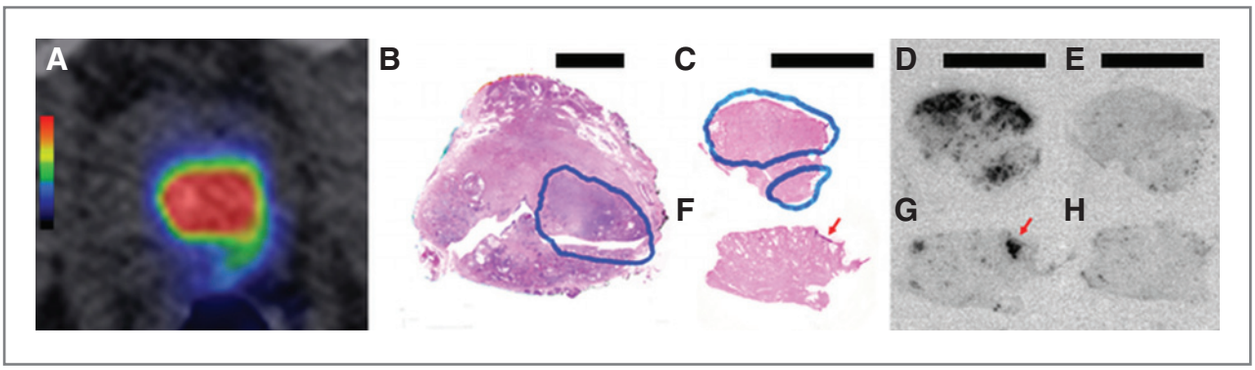

Figure 3. BAY86-7548 PET/CT (A) of patient no. 10 showing uptake in the left lobe of prostate gland in the area of cancer based on whole-mount prostatectomy sample. B, tumor is outlined in blue. Bar, 1 cm. ARG showed presence of GRPr in the section taken from the left lobe (D, top; bar, 1 cm) in the area of cancer (C, top, tumor is outlined in blue; bar, 1 cm), whereas only small areas of HGPIN in the section taken from the right lobe had positive activity (F and G, bottom, red arrow points to the area of HGPIN; bar, 1 cm). The presence of 1 mmol/L bombesin blocked uptake of [^{125}I]-Tyr^{4}-bombesin-14 in the sections from left (E, top right) and right (H, bottom right) lobe. BAY86-7548 PET/CT image is scaled to SUV, with a minimum at 0 and maximum at 5.

radiotherapy despite rapid decrease in serum PSA. In patient no. 13, BAY86-7548 was positive in one iliac and one mediastinal node, which were similarly positive on [^{11}C]-acetate. In addition, [^{11}C]-acetate showed several positive lymph nodes in unconventional locations such as axillary, parasternal, and inguinal regions. The single patient imaged in Zurich (no. 14) had multiple [^{18}F]-fluoromethylcholine–positive bone metastases and his BAY86-7548 PET/CT was totally negative.

Discussion

With the evolution of local and minimally invasive therapies for prostate cancer such as focal radiotherapy and high-intensity focused ultrasound, a pressure to develop better diagnostic tools to detect primary prostate cancer is evident. Currently, multiparametric MRI is being increasingly used in imaging of local prostate cancer to plan focal therapies (7, 8). Combination of functional and anatomic information using hybrid PET/MRI imaging can be a powerful technique provided that the applied tracer and the chosen MRI acquisition protocol are optimized for each patient individually.

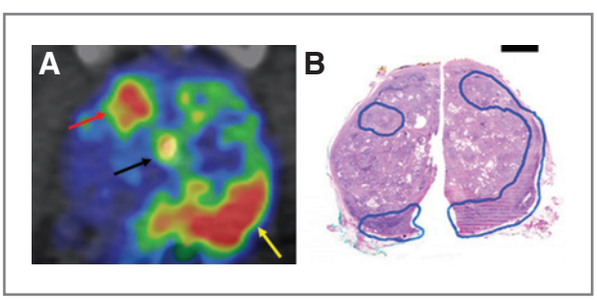

Figure 4. The uptake of BAY86-7548 in patient no. 3 was localized in the peripheral (yellow arrow in A) and central zone (red arrow in A). These areas coincide well with cancer (outlined in blue) on corresponding prostatectomy sections (B, bar, 1 cm). The large BPH nodules in the central zone did not show uptake of BAY86-7548. Black arrow points to urinary activity in a urethral catheter. The weight of the prostate gland immediately after prostatectomy was 152 g. Image is scaled to SUV, with a minimum at 0.5 and maximum at 5.

Because none of the currently available positron-emitting tracers can reliably detect early prostate cancer or identify the extent of intraprostatic disease, there is a demand for more specific tracers. An ideal tracer would detect the dominant prostate cancer lesion and differentiate cancer from BPH and inflammatory lesions. We studied a novel ^{68}Ga-labeled bombesin antagonist BAY86-7548 to translate the encouraging preclinical findings (21) to identical results in patients scheduled for radical prostatectomy or with biochemical recurrence. We were specifically interested in the uptake of BAY86-7548 in intraprostatic lesions (Fig. 4) and in the potential of the peptide tracer to detect metastatic lymph nodes. By selecting ^{68}Ga as the radionuclide, we were able to carry out the study without access to cyclotron.

The potential of ^{68}Ga-labeled peptides to target tumor receptors has been previously shown in the case of somatostatin receptor imaging. Because of their higher sensitivity and better biodistribution properties (26, 27), [^{68}Ga]-DOTATOC, [^{68}Ga]-DOTANOC, and [^{68}Ga]-DOTATATE are used for diagnosis of neuroendocrine tumors and are gradually replacing conventional gamma-emitting radioisotope techniques in Europe. In general, peptides provide excellent characteristics for PET imaging due to their easy synthesis, fast and specific targeting features, and rapid clearance from the body mainly via the renal pathway. Much like somatostatin receptors, peptides targeting G-protein–coupled receptors are effectively accumulating in tumors *in vivo*.

The GRPr, also named bombesin receptor subtype II, is a G-protein–coupled seven-transmembrane receptor belonging to the bombesin receptor family with four subtypes (for review see ref. 17). GRPr proteins are highly overexpressed in several human tumors, including prostate cancer, breast cancer, small cell lung cancer (SCLC), and non-SCLC, as well as renal cell cancer (18). Our results with radiolabeled bombesin antagonist (BAY86-7548) indicate that this tracer could be more prostate cancer-specific than imaging with [^{18}F]-, [^{11}C]-choline, or [^{11}C]-acetate, which generally

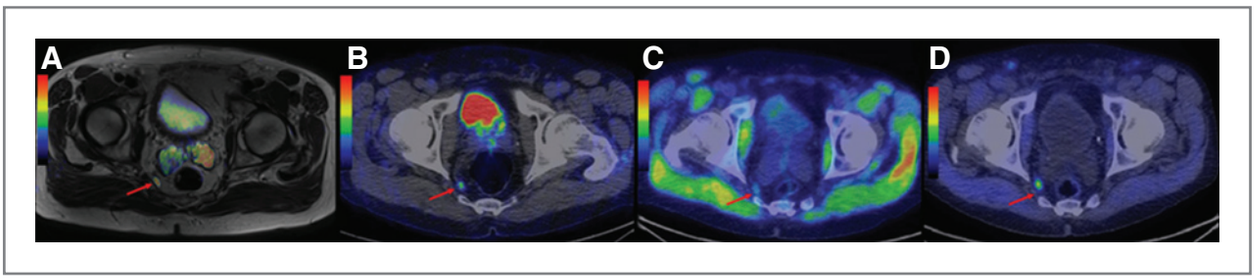

Figure 5. Preoperative fusion of diffusion-weighted imaging ($b = 750$ s/mm^2) with T2-weighted MRI (A), BAY86-7548 PET/CT (B), and [^{11}C]-acetate PET/CT (C) showed suspicious presacral metastatic lymph node in patient no. 11. BAY86-7548 SUV$_{max}$ of the node was 2.0. Unfortunately, the node could not be accessed during robotic prostatectomy and remained positive on postsurgical [^{11}C]-acetate PET/CT (D) as did the patient's PSA (1.9). The preoperative [^{11}C]-acetate SUV$_{max}$ of the suspicious node was 2.5, whereas postsurgical was 6.2. Subsequently endocrine therapy was started. Please note that uptake of [^{11}C]-acetate in pelvic muscles is not seen in BAY86-7548 PET/CT images. BAY86-7548 image is scaled to SUV, with a minimum at 0 and maximum at 5, whereas [^{11}C]-acetate images (C) and (D) are scaled to SUV, with a minimum at 0, 0 and maximum at 3.6, 10.9, respectively.

depict lipid metabolism and accumulate also in BPH and inflammatory conditions. Bombesin receptor antagonists may be preferable to agonists for tumor imaging due to higher tumor uptake and longer tumor washout time (28). In addition, bombesin receptor antagonists have reduced physiologic activity and radioactivity accumulation at physiologic GRPr targets, which potentially imply fewer side effects (28).

Despite the variety of bombesin compounds synthesized and evaluated, none have been systematically evaluated in patients with prostate cancer. The study by Van de Wiele and colleagues using [^{99m}Tc]-527RP scintigraphy targeting GRPr had only 4 patients with metastatic prostate cancer. One of these patients had specific uptake of [^{99m}Tc]-527RP in prostate cancer metastasis (29). In the current study, ^{68}Ga-labeled bombesin antagonist BAY86-7548 had encouraging results in detection of primary prostate cancer by having an accuracy of 83% for detection of the organ-confined disease. Notably, a significant difference was observed in SUV between cancerous and hyperplastic lesions. This is an encouraging finding, as non-specific uptake in benign prostatic lesions is one of the major limitations of radiolabeled choline or acetate. However, fusion of anatomic MRI with [^{18}F]-, [^{11}C]-choline, or [^{11}C]-acetate PET can only partly overcome this limitation (30). Apart from some small cancer foci, 10 of 11 dominant lesions were detected positive with BAY86-7548.

In detection of lymph node metastases, a sensitivity of 70% was observed. Although limited, it is not inferior to that seen in [^{18}F]-fluoromethylcholine, or [^{11}C]-acetate PET/CT imaging, or multiparametric MRI (Fig. 5). In addition to the lack of expression of GRPr in a particular lesion, there are two explanations for this less-than-optimal sensitivity. First, small and diffusely growing metastatic deposits or primary foci can be missed if the tumor-specific uptake is low due to partial volume effects. Second, the physical characteristics of ^{68}Ga with its average positron range between 2 and 3 mm are less ideal than those of the more widely used radionuclides such as ^{18}F (31). Because of the low number of patients with biochemical recurrence, the potential of BAY86-7548 in diagnosis of recurrent prostate cancer remained inconclusive. Finally, most of our patients undergoing a surgery belonged to the high clinical risk group with high risk of lymph node metastasis. This resulted in relatively high percentage (43%) of regions containing cancer according to histopathologic analysis and a selection bias embedded to the study inclusion criteria could not be completely avoided. Because whole-mount axial macrosections were obtained at 8-mm intervals, some small prostate cancer lesions could have been missed and the diameter of larger cancer lesions could have been underestimated. It is well known that precise correlation of prostate cancer location on whole-mount prostatectomy with PET/CT and MRI is relatively difficult (32). Anatomic landmarks, such as urethra were used to enable the correlations of whole-mount prostatectomy with PET/CT images. Although no cross-calibration of the two PET/CT scanners was conducted, the consequences are considered minimal as only 1 patient was studied using a different PET/CT scanner.

Although radiolabeled choline or acetate remain the most commonly used tracers for imaging of biochemical relapse, these tracers have shown only limited accuracy in detection of primary prostate cancer (15, 16). In a recent study, including 39 patients undergoing radical prostatectomy, multiparametric MRI showed a sensitivity of 82% for detection of prostate cancer lesions greater than 0.5 cm, whereas the sensitivity of [^{11}C]-acetate PET/CT was only 62% (33). Similarly, MRI including magnetic resonance spectroscopy has been shown to outperform [^{11}C]-choline PET/CT in evaluation of primary disease (34) and multiple studies have shown low specificity of radiolabeled choline or acetate for prostate cancer imaging due to uptake in BPH (15, 16, 33). Currently, none of these ^{18}F- or ^{11}C-labeled tracers, which are metabolized in the phospholipid synthesis pathway, can be recommended for evaluation of primary prostate cancer (35). Therefore, the 83% accuracy of BAY86-7548 PET/CT observed in this study is indeed encouraging. When combined with multiparametric MRI, BAY86-7548 PET/CT might result in sufficient diagnostic performance to allow focal treatment of intraprostatic lesions of prostate cancer.

Despite the relatively small number of patients, we have shown the feasibility of BAY86-7548 PET/CT for detection of organ-confirmed prostate cancer. Our histopathologic and ARG analyses indicated that ^{68}Ga-labeled bombesin antagonist BAY86-7548 had high prostate cancer–binding specificity with significantly higher uptake in prostate cancer compared with benign tissue. BAY86-7548 was well tolerated by all patients. This new tracer could be more accurate in detection of primary and recurrent prostate cancer than previously used positron-emitting tracers, although its feasibility in imaging of metastatic disease requires further optimization.

Disclosure of Potential Conflicts of Interest

Ray Valencia is employed as senior experimental medicine expert in Bayer Pharma AG. No potential conflicts of interest were disclosed by the other authors.

Authors' Contributions

Conception and design: E. Kähkönen, P. Luoto, M. Kallajoki, A. Roivainen, R. Valencia, H. Minn
Development of Methodology: E. Kähkönen, I. Jambor, P. Luoto, H.J. Sipilä, M. Kallajoki, A. Roivainen, R. Schibli, M. Dragic, R. Valencia, H. Minn
Acquisition of data (provided animals, acquired and managed patients, provided facilities, etc.): E. Kähkönen, J. Kemppainen, K. Lehtiö, T.J. Grönroos, A. Kuisma, P. Luoto, T. Tolvanen, K. Alanen, J. Silén, M. Kallajoki, N. Schäfer, H. Minn
Analysis and interpretation of data (e.g., statistical analysis, biostatistics, computational analysis): I. Jambor, J. Kemppainen, T.J. Grönroos, P. Luoto, J. Silén, M. Kallajoki, N. Schäfer, R. Schibli, M. Dragic, R. Valencia, H. Minn
Writing, review, and/or revision of the manuscript: E. Kähkönen, I. Jambor, J. Kemppainen, K. Lehtiö, T.J. Grönroos, A. Kuisma, P. Luoto, M. Kallajoki, A. Roivainen, R. Valencia, S. Borkowski, H. Minn
Administrative, technical, or material support (i.e., reporting or organizing data, constructing databases): T. Tolvanen, K. Alanen, M. Kallajoki, A. Johayem, R. Valencia, S. Borkowski, H. Minn
Study supervision: M. Kallajoki, R. Valencia, S. Borkowski, H. Minn

Acknowledgments

The authors thank the staff at Turku PET Centre and research nurses at the Department of Oncology and Radiotherapy and Clinical Research Service Turku (CRST), University of Turku, for their assistance; Piramal Imaging GmbH for providing the BAY86-7548 ([^{68}Ga]-DOTA-RM2), Mr. Jaakko Liippo for his help in preparing the images, and Aurexel Ltd. for editorial support. The authors also thank the European Association Nuclear Medicine (EANM) organizers for selecting the study as a recipient of the EANM Marie Curie Award.

Grant Support

This study was sponsored by Bayer Pharma AG.
The costs of publication of this article were defrayed in part by the payment of page charges. This article must therefore be hereby marked *advertisement* in accordance with 18 U.S.C. Section 1734 solely to indicate this fact.

Received November 21, 2012; revised June 28, 2013; accepted July 15, 2013; published OnlineFirst August 9, 2013.

References

1. Siegel R, Naishadham D, Jemal A. Cancer statistics, 2012. CA Cancer J Clin 2012;62:10–29.
2. Halpern EJ, Frauscher F, Strup SE, Nazarian LN, O'Kane P, Gomella LG. Prostate: high-frequency Doppler US imaging for cancer detection. Radiology 2002;225:71–7.
3. Djavan B, Ravery V, Zlotta A, Dobronski P, Dobrovits M, Fakhari M, et al. Prospective evaluation of prostate cancer detected on biopsies 1, 2, 3 and 4: when should we stop? J Urol 2001;166:1679–83.
4. Roehl KA, Antenor JA, Catalona WJ. Serial biopsy results in prostate cancer screening study. J Urol 2002;167:2435–9.
5. Rajinikanth A, Manoharan M, Soloway CT, Civantos FJ, Soloway MS. Trends in Gleason score: concordance between biopsy and prostatectomy over 15 years. Urology 2008;72:177–82.
6. Simon J, Kuefer R, Bartsch G Jr, Volkmer BG, Hautmann RE, Gottfried HW. Intensifying the saturation biopsy technique for detecting prostate cancer after previous negative biopsies: a step in the wrong direction. BJU Int 2008;102:459–62.
7. Hoeks CM, Barentsz JO, Hambrock T, Yakar D, Somford DM, Heijmink SW, et al. Prostate cancer: multiparametric MR imaging for detection, localization, and staging. Radiology 2011;261:46–66.
8. Hricak H, Choyke PL, Eberhardt SC, Leibel SA, Scardino PT. Imaging prostate cancer: a multidisciplinary perspective. Radiology 2007;243:28–53.
9. Liu IJ, Zafar MB, Lai YH, Segall GM, Terris MK. Fluorodeoxyglucose positron emission tomography studies in diagnosis and staging of clinically organ-confined prostate cancer. Urology 2001;57:108–11.
10. Takahashi N, Inoue T, Lee J, Yamaguchi T, Shizukuishi K. The roles of PET and PET/CT in the diagnosis and management of prostate cancer. Oncology 2007;72:226–33.
11. Sandblom G, Sorensen J, Lundin N, Haggman M, Malmstrom PU. Positron emission tomography with ^{11}C-acetate for tumor detection and localization in patients with prostate-specific antigen relapse after radical prostatectomy. Urology 2006;67:996–1000.
12. Oyama N, Miller TR, Dehdashti F, Siegel BA, Fischer KC, Michalski JM, et al. ^{11}C-acetate PET imaging of prostate cancer: detection of recurrent disease at PSA relapse. J Nucl Med 2003;44:549–55.
13. Wachter S, Tomek S, Kurtaran A, Wachter-Gerstner N, Djavan B, Becherer A, et al. ^{11}C-acetate positron emission tomography imaging and image fusion with computed tomography and magnetic resonance imaging in patients with recurrent prostate cancer. J Clin Oncol 2006;24:2513–9.
14. Kotzerke J, Volkmer BG, Glatting G, van den Hoff J, Gschwend JE, Messer P, et al. Intraindividual comparison of [^{11}C]acetate and [^{11}C]choline PET for detection of metastases of prostate cancer. Nuklearmedizin 2003;42:25–30.
15. Souvatzoglou M, Weirich G, Schwarzenboeck S, Maurer T, Schuster T, Bundschuh RA, et al. The sensitivity of [^{11}C]choline PET/CT to localize prostate cancer depends on the tumor configuration. Clin Cancer Res 2011;17:3751–9.
16. Jambor I, Borra R, Kemppainen J, Lepomaki V, Parkkola R, Dean K, et al. Functional imaging of localized prostate cancer aggressiveness using ^{11}C-acetate PET/CT and 1H-MR spectroscopy. J Nucl Med 2010;51:1676–83.
17. Jensen RT, Battey JF, Spindel ER, Benya RV. International Union of Pharmacology. LXVIII. Mammalian bombesin receptors: nomenclature, distribution, pharmacology, signaling, and functions in normal and disease states. Pharmacol Rev 2008;60:1–42.
18. Reubi JC, Wenger S, Schmuckli-Maurer J, Schaer JC, Gugger M. Bombesin receptor subtypes in human cancers: detection with the universal radioligand (^{125})I-[D-TYR(^{6}), beta-ALA(^{11}), PHE(^{13}), NLE(^{14})] bombesin(6-14). Clin Cancer Res 2002;8:1139–46.
19. Markwalder R, Reubi JC. Gastrin-releasing peptide receptors in the human prostate: relation to neoplastic transformation. Cancer Res 1999;59:1152–9.
20. Beer M, Montani M, Gerhardt J, Wild PJ, Hany TF, Hermanns T, et al. Profiling gastrin-releasing peptide receptor in prostate tissues: clinical implications and molecular correlates. Prostate 2012;72:318–25.
21. Mansi R, Wang X, Forrer F, Waser B, Cescato R, Graham K, et al. Development of a potent DOTA-conjugated bombesin antagonist for targeting GRPr-positive tumours. Eur J Nucl Med Mol Imaging 2011;38:97–107.
22. Reubi JC, Kvols LK, Waser B, Nagorney DM, Heitz PU, Charboneau JW, et al. Detection of somatostatin receptors in surgical and

percutaneous needle biopsy samples of carcinoids and islet cell carcinomas. Cancer Res 1990;50:5969–77.
23. Vigna SR, Mantyh CR, Giraud AS, Soll AH, Walsh JH, Mantyh PW. Localization of specific binding sites for bombesin in the canine gastrointestinal tract. Gastroenterology 1987;93:1287–95.
24. DeGroot MH, Schervish MJ. Kolmogorov–Smirnov tests. In: Probability and statistics. Pearson; 2011. London (4th ed.) p. 657–58.
25. Roivainen A, Kahkonen E, Luoto P, Borkowski S, Hofmann B, Jambor I, et al. Plasma pharmacokinetics, whole-body distribution, metabolism, and radiation dosimetry of ^{68}Ga bombesin antagonist BAY86-7548 in healthy men. J Nucl Med 2013;54:867–72.
26. Kumar R, Sharma P, Garg P, Karunanithi S, Naswa N, Sharma R, et al. Role of ^{68}Ga-DOTATOC PET-CT in the diagnosis and staging of pancreatic neuroendocrine tumours. Eur Radiol 2011;21:2408–16.
27. Ambrosini V, Campana D, Bodei L, Nanni C, Castellucci P, Allegri V, et al. ^{68}Ga-DOTANOC PET/CT clinical impact in patients with neuroendocrine tumors. J Nucl Med 2010;51:669–73.
28. Cescato R, Maina T, Nock B, Nikolopoulou A, Charalambidis D, Piccand V, et al. Bombesin receptor antagonists may be preferable to agonists for tumor targeting. J Nucl Med 2008;49:318–26.
29. Van de Wiele C, Dumont F, Vanden Broecke R, Oosterlinck W, Cocquyt V, Serreyn R, et al. Technetium-99m RP527, a GRP analogue for visualisation of GRP receptor-expressing malignancies: a feasibility study. Eur J Nucl Med 2000;27:1694–9.
30. Jambor I, Borra R, Kemppainen J, Lepomaki V, Parkkola R, Dean K, et al. Improved detection of localized prostate cancer using co-registered MRI and ^{11}C-acetate PET/CT. Eur J Radiol 2012;81:2966–72.
31. Kemerink GJ, Visser MG, Franssen R, Beijer E, Zamburlini M, Halders SG, et al. Effect of the positron range of ^{18}F, ^{68}Ga and ^{124}I on PET/CT in lung-equivalent materials. Eur J Nucl Med Mol Imaging 2011;38:940–8.
32. Meyer C, Ma B, Kunju LP, Davenport M, Piert M. Challenges in accurate registration of 3-D medical imaging and histopathology in primary prostate cancer. Eur J Nucl Med Mol Imaging 2013;40 Suppl 1:S72–8.
33. Mena E, Turkbey B, Mani H, Adler S, Valera VA, Bernardo M, et al. ^{11}C-Acetate PET/CT in localized prostate cancer: a study with MRI and histopathologic correlation. J Nucl Med 2012;53:538–45.
34. Testa C, Schiavina R, Lodi R, Salizzoni E, Corti B, Farsad M, et al. Prostate cancer: sextant localization with MR imaging, MR spectroscopy, and ^{11}C-choline PET/CT. Radiology 2007;244:797–806.
35. Picchio M, Giovannini E, Messa C. The role of PET/computed tomography scan in the management of prostate cancer. Curr Opin Urol 2011;21:230–6.